energy&fuels

Article

Cite This: Energy Fuels 2018, 32, 465−474

pubs.acs.org/EF

Ternary System of Pyrolytic Lignin, Mixed Solvent, and Water: Phase Diagram and Implications

Mingyang Li, Mingming Zhang, Yun Yu, and Hongwei Wu*

Department of Chemical Engineering, Curtin University, GPO Box U1987, Perth WA 6845, Australia

ABSTRACT: Bio-oil from biomass fast pyrolysis is considered to be an important feedstock for the production of renewable fuels and green chemicals. Fast pyrolysis bio-oil generally contains a water-soluble fraction (excluding water), a water-insoluble fraction (i.e., pyrolytic lignin, PL), and water in a single phase. However, phase separation can occur during bio-oil transport, storage, and processing. In this study, a mixed solvent (MS) is developed based on the compositions of various fast pyrolysis bio-oils produced from a wide range of feedstocks and reactor systems. Experiments are then carried out to investigate the phase behavior of the PL/MS/water ternary system. Several ternary phase diagrams are constructed for PL and its fractions, and the PL solubilities in various MS/water mixtures are also estimated. Under the experimental conditions, the PL solubility in the MS is high, i.e., ∼112 g per 100 g of MS. In the PL/MS/water system, an increase in water content to ∼17 wt % in the MS/water mixture leads to a slight increase in the PL solubility to a maximal value of ∼118 g per 100 g of MS/water mixture, followed by a gradual decrease in the PL solubility when the water content further increases. It is found that the phase stability of the PL/MS/water system is strongly determined by the composition of the system. For example, the PL/MS/water system is always stable when the MS content is >50 wt %, while the system is always phase-separated when the PL content is >54 wt %. A comparison of the results for various PL fractions indicates that the molecular weight of PL can affect the ternary phase diagram, with the PL of a lower molecular weight having a higher solubility in the same MS/water mixture. The presence of free sugar (i.e., levoglucosan, present in bio-oil as solute) also influences the ternary phase diagram of the PL/MS/system, but only at a low water content (i.e., < 20 wt %). The results suggest that such ternary diagrams may be potentially an important tool for predicting the phase separation of bio-oil, as a result of changes in the bio-oil chemistry in various processes (e.g., cold-water precipitation and aging).

1. INTRODUCTION

The world's energy consumption has been increasing substantially in the past decade, in contrast to the continuous depletion of fossil fuel reserves.[1] Fast pyrolysis is an attractive technology for converting biomass into bio-oil that is an important feedstock for producing biofuels and green chemicals.[2−5] However, bio-oil suffers from several undesired features (including high water content, high acidity, high viscosity, and phase instability) that hinder bio-oil commercial applications.[6] Phase-separated bio-oil in storage tanks may cause some serious operation problems, such as blockages, pumping difficulties, and combustion issues.[7] Therefore, understanding the phase behavior and enhancing bio-oil phase stability are important considerations.

Bio-oil is a mixture of various chemical compounds and water is the most abundant single compound that typically accounts for 15−30 wt % of bio-oil.[3] Apart from water, fast pyrolysis oil can be separated into two fractions via cold water precipitation, i.e., a water-soluble fraction (that also includes water in bio-oil) and a water-insoluble fraction that is pyrolytic lignin (PL) and of high molecular weight.[8−10] The system of water-soluble fraction (excluding water), PL, and water in fast pyrolysis bio-oil is typically in a single phase.[11] The phase stability of bio-oil is generally dictated by bio-oil compositions, which can be affected by several factors. The first factor is feedstock properties (i.e., moisture content, extractive content, ash content) that can significantly affect bio-oil phase stability.[12−14] Feedstock with a high moisture content may produce bio-oil with a higher water content, potentially leading to phase separation.[14] The second factor is pyrolysis conditions (e.g., temperature and heating rate) that can strongly affect bio-oil compositions and, hence, bio-oil phase stability. For example, while fast pyrolysis bio-oil is in a single phase, slow pyrolysis may produce phase-separated bio-oil, because of its high water content.[15,16] The third factor is the changes in bio-oil compositions during various processes. For example, aging of bio-oil typically occurs during transport and storage, leading to phase separation.[17] This is because fast pyrolysis bio-oil as a complex system is not at thermodynamic equilibrium and various chemical reactions (e.g., condensation reactions[8] and self-aggregation of reactive functional groups on PL[18]) can still proceed during storage. Therefore, phase separation of bio-oil is highly related to the proportions of water and PL.

In the open literature, the study on predicting bio-oil phase separation based on the concentrations of water, PL, and the light organic fraction is scarce. Only one study from Oasmma[7] developed a ternary phase diagram of PL, a solvent mixture (i.e., the water-soluble and ether-soluble bio-oil), and a mixture of polar components (i.e., water and sugars), and a phase stability index was developed for bio-oils. However, there are at least two limitations for that ternary phase diagram. One is that the ternary phase diagram does not cover the entire range of the three fractions. The other is that sugars should be separated from the mixture of polar components, since sugars are not solvents. Therefore, this work aims to develop a set of phase diagrams that may be suitable for predicting the phase stability of different bio-

Received: September 29, 2017
Revised: November 25, 2017
Published: November 27, 2017

DOI: 10.1021/acs.energyfuels.7b02943
Energy Fuels 2018, 32, 465−474

oils. This paper first reviews the existing data on bio-oil compositions from a wide range of feedstocks and reactor systems, and a representative mixed solvent (MS) is developed to substitute the light organic fraction of bio-oil for mixing with water and PL. Then, several ternary phase diagrams of PL (or its fraction)/MS/water system are constructed to study the phase behavior of PL and its fractions in various MS/water mixtures. The effect of free sugars (mainly levoglucosan) on the phase behavior of PL (or its fraction)/MS/water system is also investigated. The potential applications of phase diagram in predicting phase separation of bio-oil are further discussed.

2. EXPERIMENTAL SECTION

2.1. Materials. Acetic acid, hydroxyacetone, phenol, furfural, tetrahydrofuran, and methanol were purchased from Sigma−Aldrich and used without further purification, if not stated otherwise. The bio-oil sample was prepared from pinewood under fast pyrolysis conditions at 500 °C and then stored in sealed containers in the freezer at approximately −10 °C prior to experiments. The PL sample used in this study was prepared from bio-oil via cold water precipitation (following the procedure reported elsewhere[19,20]). As shown in Figure 1, the PL sample was further separated into a CH_2Cl_2-soluble fraction

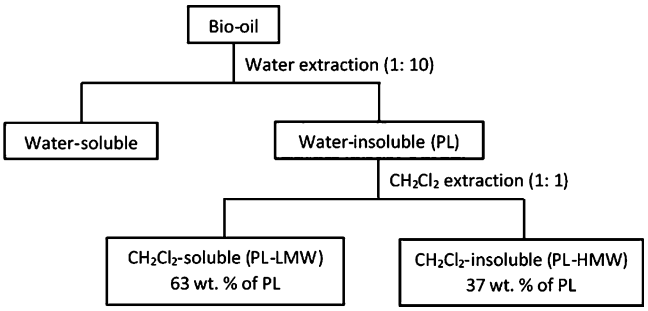

Figure 1. Preparation of pyrolytic lignin and its fractions from bio-oil.

(denoted as the "PL-LMW" sample) and a CH_2Cl_2-insoluble fraction (denoted as the "PL-HMW" sample) via CH_2Cl_2 extraction.[19,20] After extraction, the solvent was evaporated at 40 °C and the PL and its fractions were stored in a laboratory desiccator at room temperature before further experiments.

2.2. Characterization of PL and Its Fractions. A series of characterization methods were used to analyze PL and its fractions. The proximate analysis was conducted using a thermogravimetric analyzer (Mettler-Toledo Star 1). The elemental compositions of all PL samples were determined using an elemental analyzer (PerkinElmer 2400 Series II).

The UV fluorescence spectra of all PL samples were obtained using a UV fluorescence spectrometer (PerkinElmer LS 55). The analysis was carried out using synchronous scan mode with a slit width of 2.5 nm and a constant energy difference of −2800 cm^{-1}, following a method detailed elsewhere.[21] Each PL sample was dissolved in methanol to a final concentration of 10 ppm and filtered through a 0.45 μm filter paper for analysis.

Molecular weight distributions of PL and its fractions were analyzed by gel permeation chromatography (GPC), following a previous method.[22−24] Different samples were dissolved in 1000 ppm tetrahydrofuran (THF) solution, then filtered by a 0.45 μm polyvinylidene difluoride (PVDF) syringe filter (Thermo Scientific). Subsequently, the dissolved samples were analyzed by a GPC system (Varian 380-LC) equipped with an ultraviolet (UV) detector, using a set of two PLgel columns (Agilent, PLgel, 3 μm, 100 A, 300 × 7.5 mm). THF was used as the eluent at a flow rate of 1.0 mL/min for GPC analysis. Phenol and polystyrene with the molecular weight range of 94−4120 Da were used as standards.

It is known that PL contains three different types of phenolic units, i.e., guaiacyl (G), *p*-hydroxyphenyl (H), and syringyl (S), respectively.[25] The G/H/S ratios for the PL and its fractions were determined using a ^{13}C nuclear magnetic resonance (NMR) spectrometer (Bruker AV500) at 125.771 MHz according to a method detailed elsewhere.[26] In each analysis, ∼100 mg of PL (or its fractions) was dissolved in ∼0.55 mL of dimethyl sulfoxide (DMSO)-d_6. The ^{13}C NMR spectrometric data were recorded at a pulse angle of 90°, a relaxation delay of 1.5 s, and an acquisition time of 0.08 s for a total of 48 scans.

2.3. Development of Ternary Phase Diagrams. Development of ternary phase diagram follows a previous method.[27] Briefly, the experiment starts with the insoluble PL/water mixture of different concentrations, followed by progressively adding small amounts of the MS into the mixture until a homogeneous mixture is recorded with an optical microscope (Olympus SL 60/61). Since PL cannot be dissolved instantaneously, preliminary tests on a PL/MS mixture at a mass ratio of 53:47 showed that dissolution equilibrium could be reached after 30 min. UV-fluorescence spectra of dissolved fractions at various time were compared and benchmarked with that of the PL sample. Equilibrium was considered to be reached when the difference in the UV-fluorescence spectra of the dissolved fractions became negligible. When complete dissolution was achieved, the spectrum was same as that of the PL sample. Therefore, ultrasonic mixing for ∼30 min was applied in this study for each sample to ensure the dissolution equilibrium was reached. It is also noted that the phase diagrams reported in this study were constructed at room temperature (25 °C) with a standard deviation of ∼1.0% (based on weight percentage of mixed solvent in the ternary system).

3. RESULTS AND DISCUSSION

3.1. Properties of PL and Its Fractions. PLs extracted from different bio-oils can have different characteristics, in term of average molecular weight and the ratio of phenolic units.[28] It can be seen in Figure 2 that the weight-average molecular weight

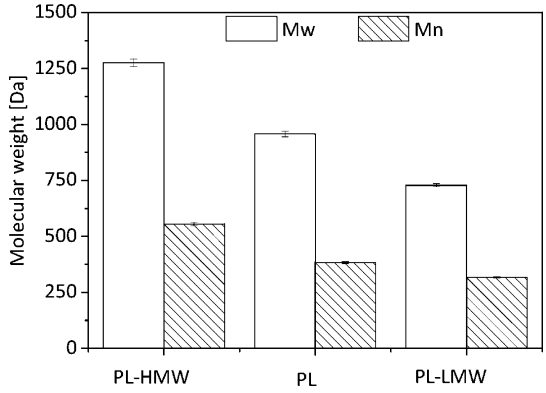

Figure 2. Weight-average molecular weight (Mw) and number-average molecular weight (Mn) of PL and its fractions. [Legend: PL-HMW, CH_2Cl_2-insoluble fraction of pyrolytic lignin; PL, pyrolytic lignin; PL-LMW, CH_2Cl_2-soluble fraction of pyrolytic lignin.]

(Mw) of the PL-HMW, PL, and PL-LMW samples are 1276, 958, and 740 Da, respectively. This is consistent with previous reported Mw values of PL from different bio-oils and PL fractions[8,9] (i.e., 650−1300 Da[9]). The proximate and ultimate analysis results of three PL samples are shown in Table 1. The PL-HMW sample has a higher fixed carbon content and a lower volatile content than the PL-LMW sample, because the PL-HMW has a much higher molecule weight and thus a lower volatility compared to the PL-LMW. Interestingly, the PL-HMW sample has a lower carbon content and a higher oxygen content than the PL-LMW sample. This leads to a higher atomic O/C ratio (0.37) and lower atomic H/C ratio (1.13) for the PL-HMW

DOI: 10.1021/acs.energyfuels.7b02943
Energy Fuels 2018, 32, 465−474

Table 1. Properties of Pyrolytic Lignin Samples

	PL-LMW[e]	PL[f]	PL-HMW[g]
moisture (wt %, ar[a])	1.1	1.8	1.8
ash (wt %, db[b])	0.6	1.5	0.9
volatile (wt %, db[b])	81.8	75.8	68.9
fixed carbon (wt %, db[b])	17.6	22.7	30.2
C (wt %, daf[c])	68.09	66.26	62.79
H (wt %, daf[c])	6.81	6.37	5.92
N (wt %, daf[c])	0.06	0.11	0.19
O (wt %, daf[c])[d]	25.04	27.26	31.1
atomic H/C	1.20	1.15	1.13
atomic O/C	0.28	0.31	0.37

[a]As received. [b]Dry basis. [c]Dry-ash-free basis. [d]By difference. [e]PL-LMW: CH_2Cl_2-soluble fraction of pyrolytic lignin. [f]PL: pyrolytic lignin. [g]PL-HMW: CH_2Cl_2-insoluble fraction of pyrolytic lignin.

sample, in comparison to 0.28 and 1.20 for the PL-LMW sample, respectively. The atomic H/C and O/C ratios are widely used for estimating fuel aromaticity and polarity, respectively.[29−31] The higher O/C ratio of the PL-HMW indicates it has a higher polarity than the PL-LMW. This is not surprising, because the PL-HMW is not soluble in CH_2Cl_2 (a nonpolar solvent) while the PL-LMW is soluble in CH_2Cl_2. The lower atomic H/C ratio of the PL-HMW suggests its higher aromaticity. The UV fluorescence intensities of all PL samples are presented in Figure 3. It can be seen that the UV fluorescence spectra of these PL

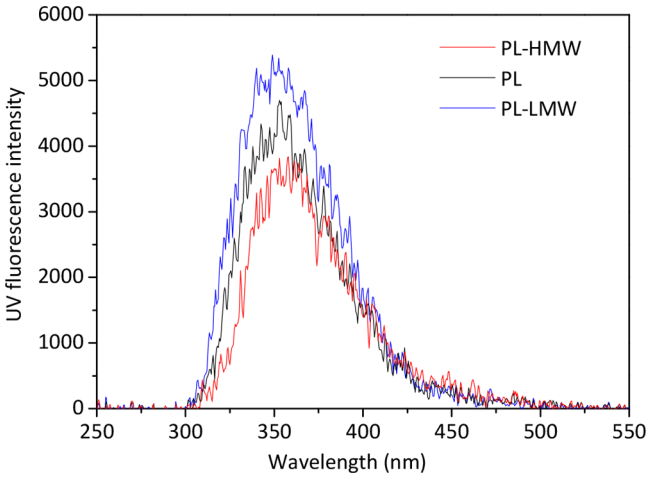

Figure 3. UV-fluorescence spectra of PL and its fractions. [Legend: PL-HMW, CH_2Cl_2-insoluble fraction of pyrolytic lignin; PL, pyrolytic lignin; PL-LMW, CH_2Cl_2-soluble fraction of pyrolytic lignin.]

samples are mainly centered at ~350 nm (corresponding to two or three fused rings[32]). The UV fluorescence spectrum of the PL-HMW slightly shifts toward larger fused-ring structures, which provides direct evidence for the higher aromaticity, as mentioned above. For the three different types of phenolic units (i.e., G, H, and S[25]), the ^{13}C NMR analysis shows that the PL, PL-HMW, and PL-LMW samples have the G/H/S ratios of 1.49/0.29/1.0, 0.81/0.1/1.0, and 1.84/0.63/1.0, respectively.

3.2. Theoretical Considerations for Formulating the MS. The MS was formulated based on major compositions of bio-oils from a wide range of feedstocks and reactor systems in the literature[21,33−49] (as listed in Table 2). The key idea is to use the MS to substitute the light organic fraction that bridges water and PL in bio-oil. Table 2 lists the light organic fraction of bio-oil, categorized into several chemical families with the respective average compositions. It can be seen that there are five major chemical families (i.e., acids, phenols, aldehydes and ketones, furans, and alcohols) that represent ~80 wt % of the light organic fraction of bio-oil (excluding PL and water). Therefore, it is possible to develop an MS based on the five major chemical families via calculating the average compositions of different chemical families on a water- and PL-free basis. To further simplify the solvent mixture, the five chemical families are represented by five model compounds (i.e., acetic acid, phenol, hydroxyacetone, furfural, and methanol) in the formulated MS. Therefore, the weight percentages of five model compounds in the MS are chosen based on the average weight percentages of each chemical family in the mixture of five major chemical families. This leads to the development of an MS with the composition of 33.3 wt % acetic acid, 33.3 wt % hydroxyacetone, 13.3 wt % phenol, 13.3 wt % furfural, and 6.8 wt % methanol.

Based on the solubility principle, "the closer the solubility parameters of the solute and the solvent are, the more likely the solubility of the solute in the given solvent",[50] PL has the maximum solubility in the MS when its solubility parameter (δ_{PL}) is close to the solubility parameter of the MS (δ_{MS}). The widely accepted rule is that the difference between the solubility parameters of the solvent and solute must be <2 $cal^{1/2}$ $cm^{-3/2}$ (i.e., the criterion $|\delta_{PL} - \delta_{MS}| \leq 2$ $cal^{1/2}$ $cm^{-3/2}$ must be satisfied).[50,51] Table 3 lists the solubility parameters of the five model compounds (as reported in the literature[50]). Therefore, based on the composition of the MS and the solubility parameter of each model compound in Table 3, the solubility parameter of the MS can be estimated, i.e., δ_{MS} = 11.99 $cal^{1/2}$ $cm^{-3/2}$. In addition, the solubility parameter of PL (or its fractions) can be calculated based on the G/H/S ratio of each sample. The solubility parameters are known for the three different types of phenolic units, i.e., δ_G = 13.52 $cal^{1/2}$ $cm^{-3/2}$ for guaiacyl, δ_H = 14.12 $cal^{1/2}$ $cm^{-3/2}$ for *p*-hydroxyphenyl, and δ_S = 14.23 $cal^{1/2}$ $cm^{-3/2}$ for syringyl.[25] Based on the G/H/S ratios reported in Section 3.1 (determined using the ^{13}C NMR method[26]), the solubility parameter of the PL, PL-HMW, and PL-LMW samples in this study are determined to be 13.84, 13.92, and 13.83 $cal^{1/2}$ $cm^{-3/2}$, respectively. To satisfy the criterion $|\delta_{PL} - \delta_{MS}| \leq 2$ $cal^{1/2}$ $cm^{-3/2}$, the solubility parameter of best solvent to dissolve the PL, PL-HMW, and PL-LMW samples should be in the range of 11.84−15.84, 11.92−15.92, and 11.83−15.83 $cal^{1/2}$ $cm^{-3/2}$, respectively. It is noteworthy that these solubility parameter ranges for the PL samples are very similar, because the differences in the solubility parameters for G, H, and S are very small (the minimum being 13.52 for δ_G and the maximum being 14.23 $cal^{1/2}$ $cm^{-3/2}$ for δ_S). It is further noted that the δ value of the formulated MS (δ_{MS} = 11.99 $cal^{1/2}$ $cm^{-3/2}$) is located within these optimum ranges, suggesting that the MS is a suitable solvent for PL dissolution. Considering the presence of water (δ_{H_2O} = 23.37 $cal^{1/2}$ $cm^{-3/2}$)[50] in bio-oil, a ternary phase diagram of PL (or its fractions)/MS/water system is further constructed. The solubilities of PL (or its fractions) in the MS/water mixtures with different water contents can be also determined.

3.3. Ternary Phase Diagram of PL/MS/Water System. Figure 4 presents the ternary phase diagram of the PL/MS/water system. The phase conversion curve clearly divides the ternary phase diagram into two regions: homogeneous region (above the curve) and inhomogeneous region (below the curve). Figures 5a and 5b illustrate the representative microscopic photographs of two PL/MS/water mixtures. Figure 5b shows a homogeneous mixture in a single phase at a PL/MS/water system with weight

DOI: 10.1021/acs.energyfuels.7b02943
Energy Fuels 2018, 32, 465−474

Table 2. Literature Data on the Compositions of Fast Pyrolysis Bio-oils[a]

fraction/main compounds	Content (wt %) dry basis	water- and PL-free basis	average content (wt %, on a water and PL free basis)	average content in five major chemical families
pyrolytic lignin	16.0−35.0	N.A.[b]	N.A.[b]	N.A.[b]
acids	12.5−25	18.5−36.5	27.5	35.0
acetic acid	3.0−15.0			
formic acid	0.9−7.6			
propionic acid	0.2−1.3			
butanoic acid	0.2−0.5			
pentanoic acid	0.1−0.8			
isocrotonic acid	0.1−1.2			
butanoic acid, 2-hydroxy-	0.1−1.0			
phenol and phenol derivates	5.0−10.0	7.5−14.5	11.0	14.0
phenol	0.1−5.0			
cresol (*o*-cresol, *m*-cresol, and *p*-cresol)	0.3−1.5			
catechol	0.6−3.0			
guaiacol	0.8−2.5			
aldehydes and ketones	8.5−25	12.5−36.5	24.5	31.5
hydroxyacetone	1.2−9.5			
glycolaldehyde (unstable, exist as dimers)	0.5−8.0			
acetaldehyde	0.1−2.0			
acetone	0.1−3.0			
linear ketones (pentanone, octanal etc.)	0.1−2.0			
cyclic ketones (C5 and C6 cyclic ketones)	0.5−5			
furan and furan derivates	5.0−10.0	7.5−14.5	11.0	14.0
furfural	1.0−5.0			
2(5H)-furanone	0.1−1.5			
furfural alcohol	0.1−1.0			
methylfurfural	0.1−0.8			
alcohols	1.0−5.0	1.5−7.5	4.5	6.0
methanol	0.5−3.5			
ethanol	0.2−1.5			
ethylene glycol	0.2−1.0			
sugars	3.0−7.0	4.5−10.0	7.3	N.A.[b]
levoglucosan	0.5−3.0			
cellobiosan	0.2−3.0			
glucose	0.4−1.3			
esters and ethers	1.0−2.0	1.5−3.0	2.3	N.A.[b]
methyl butanoate	0.1−1.3			
acetic anhydride	0.1−1.3			
methyl pyruvate	0.1−0.5			
propane, 1-ethoxy-2-methyl-	0.3−1.0			
alkene and alkane	1.0−2.0	1.5−3.5	2.5	N.A.[b]
decane	0.1−0.2			
octadecane	0.1			
2-hexene	0.1			
cyclic alkanes and alkenes	<1.0			
nitrogen compounds	<1.0	<1.0	<1.0	N.A.[b]
aniline	0.1			
pyridine	0.1			
2-hydroxypyridine	trace			
aromatics	<1.0	<1.0	<1.0	N.A.[b]
benzene	trace			
tolune	trace			
naphthalene	trace			

[a]Data taken from refs 21, 33−49. [b]N.A.: not applicable.

DOI: 10.1021/acs.energyfuels.7b02943
Energy Fuels 2018, 32, 465−474

Table 3. Composition of the Formulated MS in This Study

selected compound for the solvent	content (wt %)	solubility parameter,[a] δ ($cal^{1/2}$ $cm^{-3/2}$)
acetic acid	33.3	10.45
hydroxyacetone	33.3	13.08
phenol	13.3	11.78
furfual	13.3	12.14
methanol	6.8	14.48

[a]Data taken from ref 50.

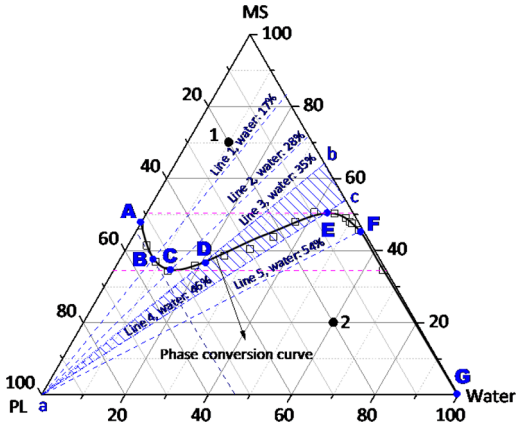

Figure 4. Ternary phase diagram of the PL/MS/water system. Line 1 represents the MS/water mixture passing through point B at which the maximal solubility of PL is achieved in the MS/water mixture. Point C represents the minimal solvent required to possibly form a homogeneous PL/MS/water solution, corresponding to line 2. Lines 3 and 4 represents the MS/water mixtures passing through points D and E, respectively, and are the boundaries of the narrow range in water content (i.e., the range of line $\overline{bc}$ of the shaded triangle *abc*) in which a drastic reduction in the solubility of PL in the MS/water mixture is evident as the content of water increases from point D to point E. Point E represents the minimal solvent at which a homogeneous solution is always formed for the ternary system, corresponding to line 4. Line 5 passes through point F, representing the MS/water mixture, which dissolves little PL. Points 1 and 2 are the representative compositions of homogeneous and inhomogeneous mixtures for microscopic photographs presented in Figures 5b and 5a, respectively. [Legend: PL, pyrolytic lignin; MS, mixed solvent.]

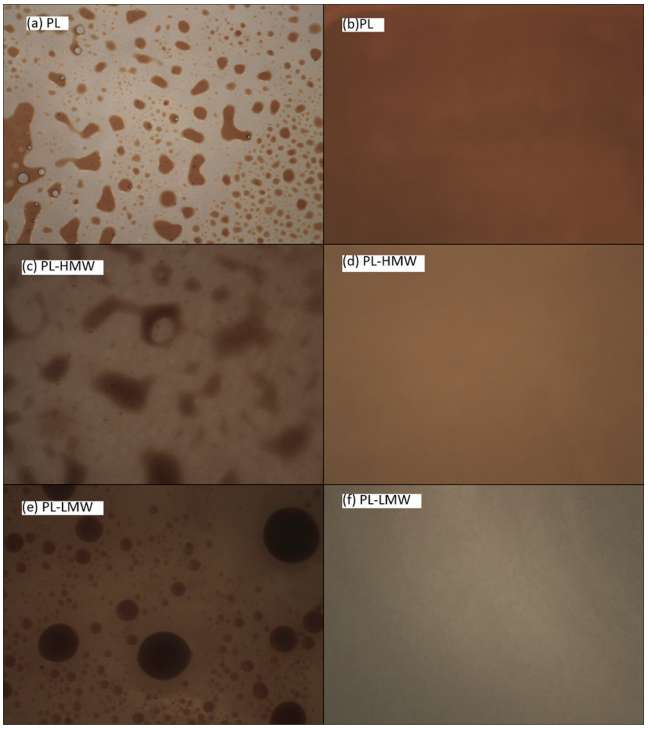

Figure 5. Representative microscopic photographs of inhomogeneous and homogeneous mixtures of PL and its fractions: (a) image of the PL/MS/water system with weight percentages of 20/20/60; (b) image of the PL/MS/water system with weight percentages of 20/70/10; (c) image of the PL/MS/water system with weight percentages of 20/20/60; (d) image of the PL-HMW/MS/water system with weight percentages of 20/70/10; (e) image of the PL-HMW/MS/water system with weight percentages of 20/20/60; and (f) image of the PL-LMW/MS/water system with weight percentages of 20/70/10. [Legend: PL-HMW, CH_2Cl_2-insoluble fraction of pyrolytic lignin; PL, pyrolytic lignin; PL-LMW, CH_2Cl_2-soluble fraction of pyrolytic lignin.]

percentages of 20/70/10, corresponding to point 1 in Figure 4. Figure 5a illustrates the heterogeneous structure of an inhomogeneous mixture at a PL/MS/water system with weight percentages of 20/20/60, corresponding to point 2 in Figure 4. The construction of the phase conversion curve in Figure 4 leads to several important points to be made.

First, considering that PL is dissolvable in the MS, it is understandable that the phase conversion curve intersects with the side (at point A) of the PL/MS binary system in Figure 4. Since PL is not dissolvable in water, the phase conversion curve does not intersect with the side of the PL/water binary system in Figure 4. Furthermore, since the MS and water are fully miscible, it is expected that the phase conversion curve intersects with the side of the MS/water binary system at the vertex "water" (i.e., point G).

Second, the datum points on the phase conversion curve in Figure 4 represent the solubilities of PL in the MS/water mixtures of various water contents. Therefore, the results on the phase conversion curve in Figure 4 can be plotted in the form of PL solubility in the MS/water mixture as a function of water content in the MS/water mixture, as shown in Figure 6a, with key points (A−F) and lines (1−5) being highlighted in both figures. In a PL/MS binary system, i.e., point A (in both Figures 4 and Figure 6a), where the water content in the MS/water mixture is zero, PL has a maximal concentration of ∼53 wt % (see Figure 4) in the PL/MS binary system, which is equivalent to a solubility of ∼112 g PL per 100 g of MS (see Figure 6a). The shift in the composition of the PL/MS/water system from point A to point B along the phase conversion curve (in Figure 4) results in an increase in water content in the PL/MS/water ternary system. As shown in both Figures 4 and 6a, increasing the water content from point A to point B enhances the solubility of PL in the MS/water mixture. However, further increasing the water content in the ternary system shifts the system from point B to point C, which witnesses a reduction in the solubility of PL in the MS/water mixture. The maximal solubility of PL in the MS/water mixture is ∼54 wt % in the PL/MS/water mixture (equivalent to the solubility of ∼118 g PL per 100 g of MS/water mixture) at point B, which corresponds to a water content of ∼17 wt % in the PL/MS/water ternary system (see line 1). Point C represents the minimal solvent (∼35 wt % in the PL/MS/water system) required to possibly form a homogeneous PL/MS/water solution, corresponding to line 2 (i.e., ∼28 wt % water in the MS/water mixture). The solubility of PL in the MS/water mixture further decreases to ∼75 g PL per 100g MS/water mixture from point C to point D, which represents the water

DOI: 10.1021/acs.energyfuels.7b02943
Energy Fuels 2018, 32, 465−474

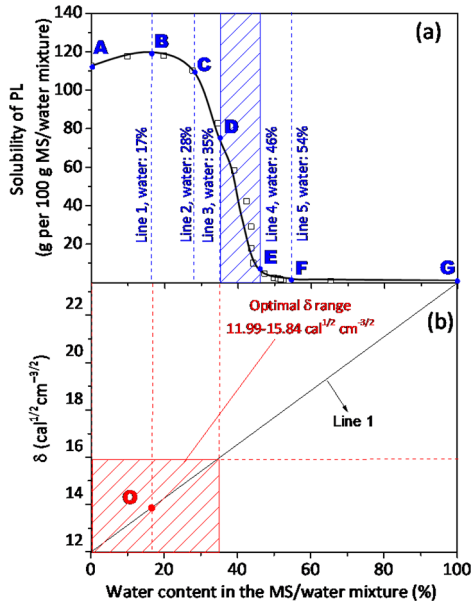

Figure 6. Solubilities of PL in various MS/water mixtures. Panel (a): lines 1−5 represent the MS/water mixtures with water contents of ∼17, ∼28, ∼35, ∼46, and ∼54 wt %, respectively; points A−G and the shaded area correspond to points A−G and the shaded triangle *abc* in Figure 4, respectively. Panel (b): line 1 represents the δ values of the MS/water mixtures at various water contents; point O represents the δ value of PL; and the shaded area represents the optimal δ range of the MS/water mixtures for the dissolution of PL. [Legend: PL, pyrolytic lignin; MS, mixed solvent.]

content of the MS/water mixture increasing from 28 wt % (line 2) to 35 wt % (line 3). However, a further shift from point D to point E, i.e., the water content of the MS/water mixture increasing from 35 wt % (line 3) to 46 wt % (line 4) results in a drastic decrease in the amount of dissolved PL in the PL/MS/water system from ∼43 wt % to ∼6 wt % (corresponding to a reduction in the PL solubility from ∼75 g per 100 g of MS/water mixture to ∼7 g per 100 g of MS/water mixture). Point E represents the minimal solvent (∼50 wt % in the PL/MS/water system) required to guarantee a homogeneous PL/MS/water solution, corresponding to line 4 (i.e., ∼46 wt % water in the MS/water mixture). When the water content in the MS/water mixture is above 54 wt % (point F, corresponding to line 5), the solubility of PL in the MS/water mixture becomes very low (<5 g per 100 g of MS/water mixture). Clearly, such a drastic reduction in the solubility of PL in the MS/water mixture demonstrates the presence of a very narrow range of water content (35−46 wt %, i.e., the range of line $\overline{bc}$ in the shaded triangle area *abc* in Figure 4 and the range in Figure 6a, bounded by lines 3 and 4) where the water content in the MS/water mixture has a critical role in dictating the solubility of PL in the MS/water mixture.

Third, the solubility principle can be used to interpret the ternary phase diagram of the PL/MS/water system. The changes in the solubility of PL in MS/water mixture can be explained via comparing the solubility parameter δ of the PL with those of the MS/water mixtures at different water contents. Figure 6b shows that the δ of the MS/water mixture increases linearly with the water content and also presents the optimal δ range (see the shaded area) of solvent for PL dissolution, according to the discussion in Section 3.2. It is interesting to note that the observed changes in the solubility of PL in MS/water mixtures (in Figures 4 and 6a) agree well with the shift in the δ value of the MS/water mixture from inside to outside of the optimal δ range in Figure 6b. The solubility of PL is high (>75 g per 100 g of MS/water mixture) in the optimal δ range (i.e., with a water content <35 wt %). Particularly, point B, which corresponds to the highest solubility of PL in the MS/water mixture and is close to line 1, which represents the MS/water mixture with a water content of ∼17 wt %, has almost the same δ value of PL. As the water content increases to >35 wt % (outside the optimal δ area), the solubility of PL in MS/water mixture decreases drastically (see Figure 6a).

Last, the ternary phase diagram provides some important guidelines for the phase stability of the PL/MS/water system. If some minimal requirements are met, the phase separation of the PL/MS/water system may be avoided. For example, the PL/MS/water system is always phase-separated, if the PL content is >54 wt %, or the water content is >54 wt %, or the MS content is <35 wt %, while the PL/MS/water system is always stable if the MS content is >50 wt %. It is also observed that the PL has good solubility (i.e., with the PL content of ∼43−54 wt %) in the MS/water mixture, if the water content in the MS/water mixture is <35 wt %. There is also a critical range (i.e., 35−46 wt %) of the water content in the MS/water mixture, where the PL solubility is drastically affected by the water content.

3.4. Ternary Phase Diagrams of PL-HMW/MS/Water and PL-LMW/MS/Water Systems. The ternary phase diagrams of different PL fractions were further developed to understand the phase behavior of different PL fractions in the MS/water mixtures. The ternary phase diagrams and the solubilities of the PL-HMW and PL-LMW are compared in Figures 7 and 8. The representative microscopic photographs for the PL-HMW and PL-LMW are also shown in Figures 5c−f. Two important observations can be made. One is the solubilities of different PL fractions in the same MS/water mixture follow an order of PL-LMW > PL > PL-HMW. The PL-LMW shows a much higher solubility in the same MS/water mixture, compared to other PL fractions. It appears that the solubility of PL (or its fractions) is strongly influenced by the average molecular weight, with an increased solubility for PL of a lower average molecular weight. Thus, the PL-LMW can maintain a single phase in the MS/water mixture with a lower MS content and/or a higher water content, in comparison to PL and PL-HMW. For example, the PL-LMW/MS/water system is always stable if the MS content is >48 wt %, in comparison to >54 and >57 wt % for the PL/MS/water and PL-HMW/MS/water systems, respectively. The results suggest that the bio-oil phase stability can be largely improved if the content of PL-HMW in the bio-oil is low, and solvent addition is an effective strategy to improve the bio-oil stability.

The other important observation is that the trends of the phase conversion curves for PL fractions follow a similar pattern to that for the PL, as highlighted with similar key points (A−F) and lines (1−5) in Figure 7 (also plotted as the solubilities of PL factions in the MS/water mixture in Figure 8). In PL-HMW/MS or PL-LMW/MS binary systems, the PL-HMW and PL-LMW has maximal concentrations of ∼45 and ∼58 wt % in the binary systems, as shown in Figure 7, corresponding to the solubility of ∼85 and ∼138 g per 100 g of MS, respectively. As the composition of the ternary mixture shifts from point A to point B along the phase conversion curve (see Figures 7a and 7b), the increase of a small amount of water also enhances the solubility of the PL-HMW or PL-LMW in the MS/water mixture. For example, the PL-HMW and PL-LMW have maximal concentrations of ∼49 and ∼61 wt % in the ternary system,

DOI: 10.1021/acs.energyfuels.7b02943
Energy Fuels 2018, 32, 465−474

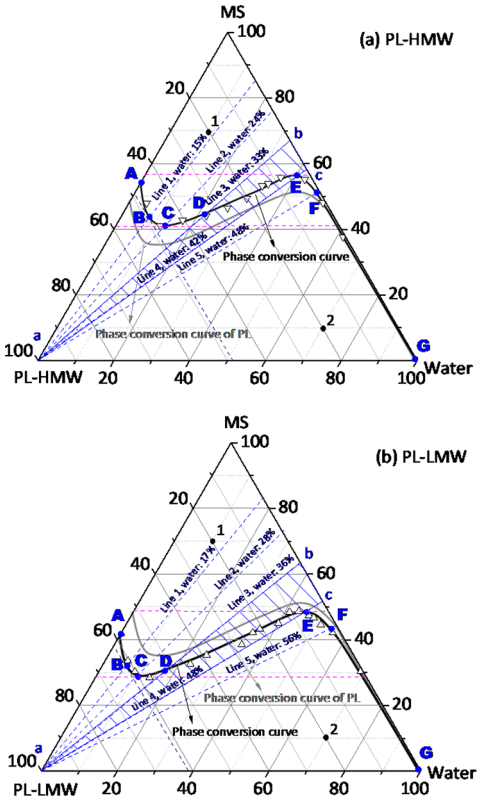

Figure 7. Ternary phase diagrams of PL-HMW/MS/water and PL-LMW/MS/water: (a) lines 1−5 represent the MS/water mixtures with a water content of ∼15, ∼24, ∼33, ∼42, and ∼48 wt %, respectively; (b) line 1−5 represent the MS/water mixtures with a water content of ∼17%, ∼28%, ∼36%, ∼49%, and ∼56%, respectively. Definitions of lines 1−5 and the shaded area *abc* in both panels (a) and (b) are same as those given in Figure 4. Points 1 and 2 in both panels are the representative compositions of homogeneous and inhomogeneous mixtures for microscopic photographs presented in Figure 5d,f and 5c,e, respectively. [Legend: PL-HMW, CH_2Cl_2 insoluble fraction of pyrolytic lignin; PL-LMW, CH_2Cl_2 soluble fraction of pyrolytic lignin; MS, mixed solvent.]

corresponding to water contents of ∼15 and ∼17 wt % (line 1 in Figures 7a, 7b, 8a, and 8b) in the MS/water mixtures, respectively. This is equivalent to the solubilities of ∼96 and ∼156 g per 100 g of MS/water mixture (see Figures 8a and 8b), respectively. Similar as the PL/MS/water phase diagram, further increasing of water content (from point B to point C) in the MS/water mixture results in a reduction in the solubilities of PL-HMW and PL-LMW in the MS/water mixture. At point C, the minimal MS required to homogenize the PL-HMW/MS/water and PL-LMW/MS/water mixture is ∼42 and ∼29 wt %, respectively (see line 2 in Figure 7a, 7b, 8a, and 8b). The solubilities of the PL-HMW and PL-LMW in the MS/water mixture continue to decrease to ∼50 g of PL-HMW and ∼120 g of PL-LMW per 100 g MS/water mixture from point C to point D. Shifting from point D to point E represents the water content of MS/water mixture for the PL-HMW and PL-LMW increasing from 33 to 42 wt % and from 36 to 49 wt %, respectively. Within such narrow ranges (as shown in Figures 8a and 8b), the solubilities of PL-HMW and PL-LMW decrease drastically from ∼44 g per 100 g of MS/water mixture to ∼3 g per 100 g of MS/water mixture and from ∼120 g per 100 g of MS/water mixture to ∼6 g per 100 g of MS/water mixture, respectively. When the water content in the PL-HMW/MS/water and PL-LMW/MS/water system is >48 and >56 wt % (point F in Figures 7a and 7b), the solubilities of PL-HMW and PL-LMW in the MS/water mixture approach almost zero.

The data on the solubilities of the PL-HMW and PL-LMW presented in Figures 7a, 7b, 8a, and 8b can also be interpreted based on the solubility principles. The δ values of the PL-HMW and PL-LMW are 13.92 and 13.83, respectively. At point B, where the maximal solubilities of PL-HMW and PL-LMW are reached, the δ values of the MS/water mixtures (with 15 and 17 wt % of water in the MS/water mixture, corresponding to line 1 in Figures 7a, 7b, 8a, and 8b) are 13.7 and 13.9 (see Figures 8c and 8d), respectively. Therefore, the δ values of the MS/water mixtures closely match those of the solutes (PL-HMW or PL-LMW), as shown Figure 8. Similarly, it is also understandable for the presence of the critical ranges in the water content (i.e., ∼33−42 wt % for the PL-HMW and ∼36−49 wt % for the PL-LMW from point D to point E) of the MS/water mixtures, where the solubilities of the PL-HMW and PL-LMW are drastically affected by the water content. This is because, as the water content of the MS/water mixture increases to that of point D (i.e., ∼33 and ∼36 wt % for the PL-HMW and PL-LMW), the δ values of the MS/water mixtures move out of the optimal δ ranges for the dissolution of the PL-HMW and PL-LMW, respectively. At point E (i.e., ∼42 and ∼49 wt % water in the MS/water mixture for the PL-HMW and PL-LMW), the δ values of the MS/water mixtures are far beyond the optimal δ ranges for dissolving the PL-HMW or PL-LMW, the solubilities of PL fractions become very low (<5 g per 100 g of MS/water mixture).

3.5. Effect of Sugar on Ternary Phase Diagrams of PL and Its Fractions. Bio-oil can be considered as a mixture of three pseudo-components: PL, water-soluble fraction (excluding water), and water. In this study, the water-soluble fraction is modeled by the MS that is formulated from the five model compounds representing the five key chemical families (i.e., acids, phenols, aldehydes and ketones, furans, and alcohols). As shown in Table 2, sugar is another important solute in the bio-oil system, in addition to PL. Therefore, to enable the practical application of the PL/MS/water ternary phase diagram, the effect of sugar on the phase behavior of the ternary systems should be studied. It is important to note that the sugar as a solute refers to the free sugar in the system. It was recently reported[20] that ∼5−7 wt % of sugar (mainly in the form of levoglucosan) could be present in the bio-oil used in this study. Therefore, levoglucosan was added into the PL/MS/water systems at two different contents of 5 and 7 wt % (calculated based on the entire system containing PL, MS, water and the added levoglucosan) to evaluate the effect of sugar on the phase behavior of the PL/MS/water ternary system and generate the phase conversion curves. To evaluate the effect of levoglucosan, the ternary diagram is plotted on a levoglucosan-free basis, i.e., the contents of PL, MS and water normalized to 100% for the PL/MS/water ternary system, excluding levoglucosan that has been added into the system. Similar phase diagrams are also developed and constructed for the PL-HMW/MS/water and PL-LMW/MS/water systems, as shown in Figure 9.

Figure 9 shows that the phase conversion curves of the PL (or its fraction)/MS/water systems can be greatly affected by the presence of levoglucosan in the system when the water content in the ternary system is low (i.e., < 20 wt %). For example, when levoglucosan is added in the PL/MS binary system at a content of 5% in the entire mixture, the maximal PL content in the PL/MS binary system for forming a homogeneous system reduces significantly from 53 wt % to 37 wt % (on a levoglucosan-free

DOI: 10.1021/acs.energyfuels.7b02943
Energy Fuels 2018, 32, 465−474

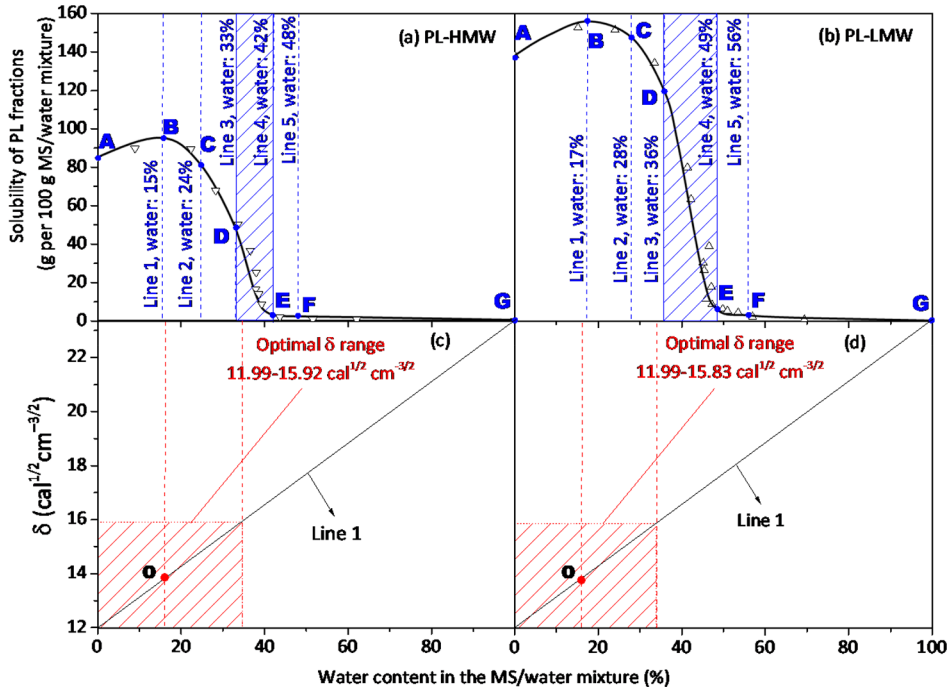

Figure 8. Solubilities of PL-HMW/MS/water and PL-LMW/MS/water in various MS/water mixtures: (a) lines 1−5 represent the MS/water mixture with a water content of ∼15, ∼24, ∼33, ∼42, and ∼48 wt %, respectively; (b) lines 1−5 represent the MS/water mixture with a water content of ∼17, ∼28, ∼36, ∼49, and ∼56 wt %, respectively: (c and d) line 1 represents the δ values of the MS/water mixtures at various water contents; point O represents the δ value of PL-HMW (or PL-LMW); and the shaded area represents the optimal δ ranges of the MS/water mixtures for the dissolution of PL-HMW (or PL-LMW). Points A−G in panel (a) and (b) correspond to points A−G in Figure 7a and 7b, respectively. The shaded areas in panel (a) and (b) correspond to the shaded triangles *abc* in Figure 7a and 7b, respectively. Definitions of lines 1−5 in panels (a) and (b) are same as those given in Figure 4. Definitions of shaded areas in panels (a) and (b) are same as that in Figure 6. [Legend: PL-HMW, CH_2Cl_2 insoluble fraction of pyrolytic lignin; PL-LMW, CH_2Cl_2 soluble fraction of pyrolytic lignin; MS, mixed solvent.]

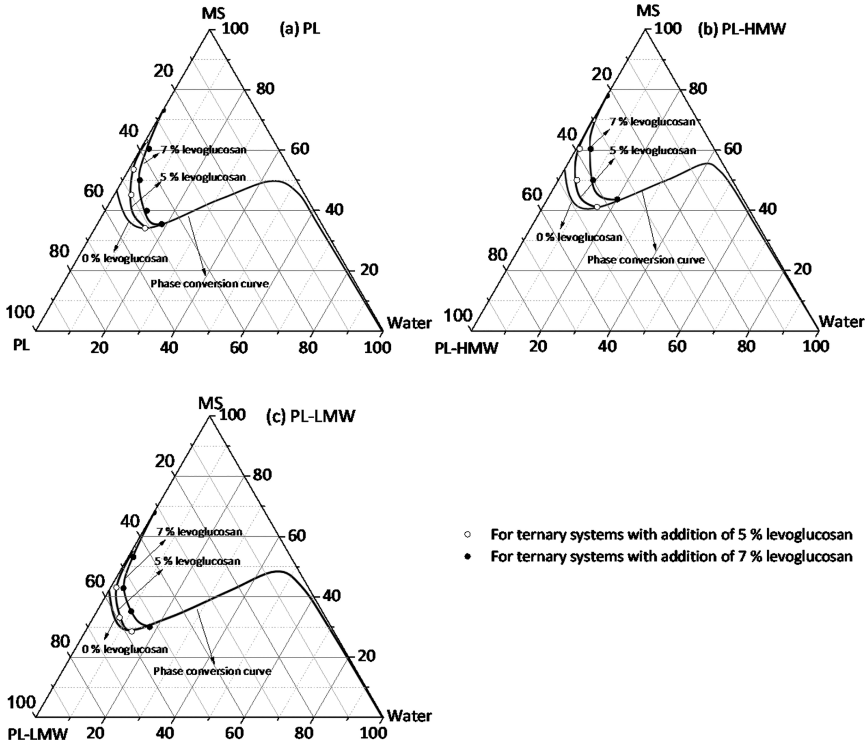

Figure 9. Ternary phase diagrams of the PL (its fraction)/MS/water system with the contents of sugar (represented by levoglucosan) being 5 and 7 wt % in the overall systems, respectively. The ternary diagrams are plotted with the contents of PL (or its fraction), MS, and water normalized to 100% (excluding sugar in the system). [Legend: PL, pyrolytic lignin; PL-HMW, CH_2Cl_2 insoluble fraction of pyrolytic lignin; PL-LMW, CH_2Cl_2 soluble fraction of pyrolytic lignin; MS, mixed solvent.]

DOI: 10.1021/acs.energyfuels.7b02943
Energy Fuels 2018, 32, 465−474

basis). Meanwhile, the maximal solubilities for the PL-HMW and PL-LMW in the PL fraction/MS binary system decrease from ~45 wt % to 30 wt % and from ~58 wt % to 44 wt % (on a levoglucosan-free basis), respectively. An increase in the content of levoglucosan to 7 wt % in the entire mixture further reduces the maximal contents of the PL, PL-HMW, and PL-LMW to ~25, 22, and 32 wt %, respectively. However, the maximal contents of the PL, PL-HMW, and PL-LMW increase substantially as the water content in the PL(PL-HMW or PL-LMW)/MS/water ternary system increases. The more sugar added into the system, the more water required to keep the system homogeneous. When the water content in the ternary system (on a levoglucosan-free basis) is higher than a certain value (i.e., >15 wt % and >20 wt % at 5 wt % and 7 wt % of levoglucosan in the entire mixture, respectively), the sugar has no effect on the solubility of PL (or its fractions) in the MS/water mixture, hence the ternary phase diagrams of the PL/MS/water, PL-HMW/MS/water, and PL-LMW/MS/water systems.

3.6. Applications of the Ternary Phase Diagram. To test the applicability of the phase diagram, the data on the bio-oils with known composition of PL, MS, water, and sugar are required. In the process of collecting literature, three important considerations are taken into account. First, the importance of free sugar in the system must be considered. Therefore, only the bio-oil samples in the previous studies[20,52−54] that reported free sugars contents of <7 wt % are included. Second, fast pyrolysis bio-oil concerns PL in the system, so the collected literature data are replotted in the ternary phase diagram of the PL/MS/water system. Third and last, the literature data are processed and converted to be on a sugar-free basis for plotting on the phase diagram. As shown in Figure 10, coincidently, all the bio-oil

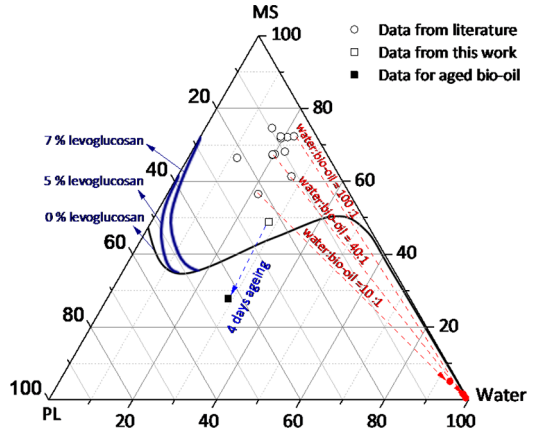

Figure 10. Practical applications of the phase diagram for predicting the phase stability of bio-oil samples with known compositions from the literature.[20,52−54] The ternary diagram is plotted with the contents of PL, MS, and water normalized to 100% (excluding sugar in the system). The three red dashed lines represent the cold water precipitation process at water/bio-oil ratios of 10/1, 40/1, and 100/1, respectively.[20,53,54] The blue dashed line represents a 4-day bio-oil accelerated aging process at 80 °C. [Legend: PL, pyrolytic lignin; MS, mixed solvent.]

samples with known compositions are within the homogeneous region of the PL/MS/water phase diagram at 7 wt % levoglucosan in the entire system. It appears that such a ternary phase diagram of the PL/MS/water system may be useful in predicting the phase stability of bio-oil samples.

It is known that bio-oil can be separated into two phases with excess water content.[55] This process can be clearly reflected in the phase diagram. In this study, a single-phase bio-oil was added into cold water with different water-to-oil ratios ranging between 10 and 100, a two-phase bio-oil was easily formed even at a low water-to-oil ratio of 10. Therefore, it is clear that bio-oil experiences phase separation after being added into excess cold water. However, bio-oils with different PL-to-MS ratios require different amounts of water for phase separation. The phase conversion curve in Figure 10 indicates that, when the water content is above ~40 wt %, phase separation can easily occur for most bio-oils.

Moreover, the aging process of fast pyrolysis bio-oil can also be reflected in the ternary phase diagram. In this study, an accelerated aging experiment of the bio-oil sample was also carried out at 80 °C for 4 days to generate experimental data for plotting in the phase diagram, since relevant experimental data are unavailable in the literature. As clearly shown in Figure 10, the bio-oil sample experienced phase separation after aging, because of the drastic increase in the PL content in the aged bio-oil sample. It suggests that the bio-oil sample experienced irreversible composition changes, especially leading to significant increase in the PL content. Therefore, such ternary phase diagrams can be very useful in predicting the bio-oil aging process. Based on the phase diagram, it may also be possible to estimate the amount of solvent required to be added into bio-oil system for avoiding the phase separation during bio-oil storage.

4. CONCLUSIONS

In this paper, a mixed solvent (MS) is developed based on the composition of bio-oils in the existing literature for studying the phase behavior of PL/MS/water ternary system. Several ternary phase diagrams of PL/MS/water systems are constructed for PL and its fractions, and their solubilities in various MS/water mixtures are also estimated. The phase stability of the PL/MS/water system is strongly determined by the composition of the ternary system. For example, the PL/MS/water system is always phase-separated, if the PL content is >54 wt %, or the water content is >54 wt %, or the MS content is <35 wt %, while the PL/MS/water system is always stable if the MS content is >50 wt %. The ternary phase diagram can be successfully interpreted by the solubility principle. The PL solubility is high in the PL/MS binary system. An increase in the water content first leads to a slight increase in the PL solubility, followed by a gradual decrease as the water content further increases. However, there is a narrow water content range where the PL solubility is significantly affected by the water content in the ternary system, i.e., 43−54 wt % for the PL. The solubilities of different PL fractions indicate that PL solubility is influenced by its average molecular weight, and the PL of a lower average molecular weight has a higher solubility in the same MS/water mixture. The presence of free sugar (i.e., levoglucosan) also affects the phase stability of the PL/MS/water system, but only at low water content (i.e., <20 wt %). A higher sugar content leads to the phase separation of the PL/MS/system at a lower PL content. The results suggest that the ternary phase diagram of the PL/MS/water system can be a powerful tool in predicting phase separation of bio-oil in various processes such as water precipitation and aging.

AUTHOR INFORMATION

Corresponding Author

*Fax: +61-8-92662681. E-mail: h.wu@curtin.edu.au.

ORCID

Hongwei Wu: 0000-0002-2816-749X

DOI: 10.1021/acs.energyfuels.7b02943
Energy Fuels 2018, 32, 465−474

Notes

The authors declare no competing financial interest.

■ ACKNOWLEDGMENTS

The work is partially supported by the Australian Research Council via its Discovery Projects scheme. M.L. also sincerely acknowledges the CIPRS Scholarship received from Curtin University.

■ REFERENCES

(1) *BP Statistical Review of World Energy*; BP: London, U.K., 2017.
(2) Bridgwater, A. V. *Chem. Eng. J.* **2003**, *91* (2−3), 87−102.
(3) Czernik, S.; Bridgwater, A. V. *Energy Fuels* **2004**, *18* (2), 590.
(4) Solantausta, Y.; Oasmaa, A.; Sipilä, K.; Lindfors, C.; Lehto, J.; Autio, J.; Jokela, P.; Alin, J.; Heiskanen, J. *Energy Fuels* **2012**, *26* (1), 233−240.
(5) Xu, W.; Gao, L.; Wang, S.; Xiao, G. *Energy Fuels* **2013**, *27* (11), 6738−6742.
(6) Meng, J.; Moore, A.; Tilotta, D. C.; Kelley, S. S.; Adhikari, S.; Park, S. *Energy Fuels* **2015**, *29* (8), 5117−5126.
(7) Oasmaa, A.; Sundqvist, T.; Kuoppala, E.; Garcia-Perez, M.; Solantausta, Y.; Lindfors, C.; Paasikallio, V. *Energy Fuels* **2015**, *29* (7), 4373−4381.
(8) Oasmaa, A.; Kuoppala, E. *Energy Fuels* **2003**, *17* (4), 1075.
(9) Scholze, B.; Hanser, C.; Meier, D. *J. Anal. Appl. Pyrolysis* **2001**, *58*−*59*, 387−400.
(10) Scholze, B.; Meier, D. *J. Anal. Appl. Pyrolysis* **2001**, *60* (1), 41.
(11) Oasmaa, A.; Fonts, I.; Pelaez-Samaniego, M. R.; Garcia-Perez, M. E.; Garcia-Perez, M. *Energy Fuels* **2016**, *30* (8), 6179−6200.
(12) Elliott, D. C. *Biomass Bioenergy* **1994**, *7* (1−6), 179−185.
(13) Fahmi, R.; Bridgwater, A. V.; Darvell, L. I.; Jones, J. M.; Yates, N.; Thain, S.; Donnison, I. S. *Fuel* **2007**, *86* (10−11), 1560−1569.
(14) Peacocke, G. V. C.; Russell, P. A.; Jenkins, J. D.; Bridgwater, A. V. *Biomass Bioenergy* **1994**, *7* (1−6), 169−177.
(15) Wang, X.; Kersten, S. R. A.; Prins, W.; van Swaaij, W. P. M. *Ind. Eng. Chem. Res.* **2005**, *44* (23), 8786−8795.
(16) Zhou, S.; Garcia-Perez, M.; Pecha, B.; Kersten, S. R. A.; McDonald, A. G.; Westerhof, R. J. M. *Energy Fuels* **2013**, *27* (10), 5867−5877.
(17) Yu, F.; Deng, S.; Chen, P.; Liu, Y.; Wan, Y.; Olson, A.; Kittelson, D.; Ruan, R. *Appl. Biochem. Biotechnol.* **2007**, *137* (1), 957−970.
(18) Fratini, E.; Bonini, M.; Oasmaa, A.; Solantausta, Y.; Teixeira, J.; Baglioni, P. *Langmuir* **2006**, *22* (1), 306−312.
(19) Chua, Y. W.; Yu, Y.; Wu, H. *Fuel* **2017**, *200*, 70−75.
(20) Yu, Y.; Chua, Y. W.; Wu, H. *Energy Fuels* **2016**, *30* (5), 4145.
(21) Stankovikj, F.; McDonald, A. G.; Helms, G. L.; Olarte, M. V.; Garcia-Perez, M. *Energy Fuels* **2017**, *31* (2), 1650−1664.
(22) Kim, J.-Y.; Oh, S.; Hwang, H.; Kim, U.-J.; Choi, J. W. *Polym. Degrad. Stab.* **2013**, *98* (9), 1671−1678.
(23) McClelland, D. J.; Motagamwala, A. H.; Li, Y.; Rover, M. R.; Wittrig, A. M.; Wu, C.; Buchanan, J. S.; Brown, R. C.; Ralph, J.; Dumesic, J. A.; Huber, G. W. *Green Chem.* **2017**, *19* (5), 1378−1389.
(24) Nair, V.; Vinu, R. *J. Anal. Appl. Pyrolysis* **2016**, *119*, 31−39.
(25) Wang, Q.; Chen, K.; Li, J.; Yang, G.; Liu, S.; Xu, J. *BioResources* **2011**, *6* (3), 3034−3043.
(26) Yuan, T.-Q.; Sun, S.-N.; Xu, F.; Sun, R.-C. *J. Agric. Food Chem.* **2011**, *59* (12), 6605−6615.
(27) Zhang, M.; Wu, H. *Energy Fuels* **2014**, *28* (7), 4650−4656.
(28) Azadi, P.; Inderwildi, O. R.; Farnood, R.; King, D. A. *Renewable Sustainable Energy Rev.* **2013**, *21*, 506−523.
(29) Li, H.; Qu, R.; Li, C.; Guo, W.; Han, X.; He, F.; Ma, Y.; Xing, B. *Bioresour. Technol.* **2014**, *163*, 193−198.
(30) Ray, P. Z.; Chen, H.; Podgorski, D. C.; McKenna, A. M.; Tarr, M. A. *J. Hazard. Mater.* **2014**, *280*, 636−643.
(31) Ahmad, M.; Lee, S. S.; Dou, X.; Mohan, D.; Sung, J.-K.; Yang, J. E.; Ok, Y. S. *Bioresour. Technol.* **2012**, *118*, 536−544.
(32) Wang, Y.; Li, X.; Mourant, D.; Gunawan, R.; Zhang, S.; Li, C.-Z. *Energy Fuels* **2012**, *26* (1), 241−247.
(33) Diebold, J. P. *A Review of the Chemical and Physical Mechanisms of the Storage Stability of Fast Pyrolysis Bio-oils*; National Renewable Energy Laboratory: Golden, CO, 1999.
(34) Mohan, D.; Pittman, C. U.; Steele, P. H. *Energy Fuels* **2006**, *20* (3), 848−889.
(35) Yanik, J.; Kornmayer, C.; Saglam, M.; Yüksel, M. *Fuel Process. Technol.* **2007**, *88* (10), 942−947.
(36) Zhang, Q.; Chang, J.; Wang, T.; Xu, Y. *Energy Convers. Manage.* **2007**, *48* (1), 87−92.
(37) Zheng, J.-l. *J. Anal. Appl. Pyrolysis* **2007**, *80* (1), 30−35.
(38) Ingram, L.; Mohan, D.; Bricka, M.; Steele, P.; Strobel, D.; Crocker, D.; Mitchell, B.; Mohammad, J.; Cantrell, K.; Pittman, C. U. *Energy Fuels* **2008**, *22* (1), 614−625.
(39) Jung, S.-H.; Kang, B.-S.; Kim, J.-S. *J. Anal. Appl. Pyrolysis* **2008**, *82* (2), 240−247.
(40) Das, D. D.; Schnitzer, M. I.; Monreal, C. M.; Mayer, P. *Bioresour. Technol.* **2009**, *100* (24), 6524−6532.
(41) Heo, H. S.; Park, H. J.; Dong, J.-I.; Park, S. H.; Kim, S.; Suh, D. J.; Suh, Y.-W.; Kim, S.-S.; Park, Y.-K. *J. Ind. Eng. Chem.* **2010**, *16* (1), 27−31.
(42) Oasmaa, A.; Peacocke, C. *Properties and Fuel Use of Biomass-Derived Fast Pyrolysis Liquids: A Guide*; VTT Publication *731*; VTT Publications: Espoo, Finland, 2010, *731*, 79.
(43) Chen, T.; Wu, C.; Liu, R.; Fei, W.; Liu, S. *Bioresour. Technol.* **2011**, *102* (10), 6178−6185.
(44) Guo, X.; Wang, S.; Wang, Q.; Guo, Z.; Luo, Z. *Chin. J. Chem. Eng.* **2011**, *19* (1), 116−121.
(45) Bertero, M.; de la Puente, G.; Sedran, U. *Fuel* **2012**, *95*, 263.
(46) Oasmaa, A.; Källi, A.; Lindfors, C.; Elliott, D. C.; Springer, D.; Peacocke, C.; Chiaramonti, D. *Energy Fuels* **2012**, *26* (6), 3864−3873.
(47) Hu, Z.; Zheng, Y.; Yan, F.; Xiao, B.; Liu, S. *Energy* **2013**, *52*, 119−125.
(48) Alvarez, J.; Lopez, G.; Amutio, M.; Bilbao, J.; Olazar, M. *Fuel* **2014**, *128*, 162−169.
(49) Artigues, A.; Puy, N.; Bartrolí, J.; Fábregas, E. *Energy Fuels* **2014**, *28* (6), 3908−3915.
(50) Hansen, C. M. *Hansen Solubility Parameters: A User's Handbook*; CRC Press: Boca Raton, FL, 2007.
(51) Ye, Y.; Liu, Y.; Chang, J. *BioResources* **2014**, *9* (2), 3417.
(52) Zhou, S.; Mourant, D.; Lievens, C.; Wang, Y.; Li, C.-Z.; Garcia-Perez, M. *Fuel* **2013**, *104*, 536−546.
(53) Liaw, S.-S.; Wang, Z.; Ndegwa, P.; Frear, C.; Ha, S.; Li, C.-Z.; Garcia-Perez, M. *J. Anal. Appl. Pyrolysis* **2012**, *93*, 52−62.
(54) Mourant, D.; Wang, Z.; He, M.; Wang, X. S.; Garcia-Perez, M.; Ling, K.; Li, C.-Z. *Fuel* **2011**, *90* (9), 2915−2922.
(55) Oasmaa, A.; Koponen, P. *Physical Characterisation of Biomass-Based Pyrolysis Liquids*; Espoo, Finland, 1997.

DOI: 10.1021/acs.energyfuels.7b02943
Energy Fuels 2018, 32, 465−474